Babes-Bolyai University

Faculty of Physics

Doctoral Thesis Summary

Gelatin-coated and drug-loaded gold nanoparticles for performing therapeutic and multimodal imaging functionalities

by

Sorina-Maria Suărăşan

Scientific Advisor
Prof. Dr. Simion Aştilean

CLUJ-NAPOCA
2015

Table of contents

Thesis outline

The major aim of this thesis is to design new plasmonic gold nanoparticles (AuNPs) as multimodal effective biomedical agents. We focused on two major applications of AuNPs: in regenerative medicine and cancer therapy.

My thesis is structured into three main parts containing six chapters. **Part I**, entitled Introduction and Review of related literature consist of **Chapter 1** which presents a short review of the scientific literature focused on the gold nanoparticles synthesis methods, properties and biomedical applications.

The following chapters of **Part II** presents the results obtained during my PhD stage in the *Nanobiophotonics Center* of the *Interdisciplinary Research Institute in Bio-Nano-Sciences* from Babes-Bolyai University in collaboration with *Radiobiology and Tumor Biology Laboratory* from *Oncological Institute "Prof. Dr. Ion Chiricuţă",* Cluj-Napoca, Romania.

Chapter 2 present an environmentally friendly approach for the stabilization and biocompatibilization of citrate-reduced AuNPs in aqueous solution, to improve their properties and biomedical applications. We obtained two classes of bioconjugates: one operational as highly sensitive surface-enhanced Raman scattering (SERS) active substrate and the other one useful as platforms for loading of different FLT3 inhibitors, drugs employed in leukemia treatment.

In **Chapter 3**, in order to combine unique properties of AuNPs with functionality of gelatin, but without using any relatively toxic reducing agents and surfactants, we propose a new method to biosynthesize AuNPs. Taking the advantage of gelatin biopolymer to operate as unique reducing, growth controlling and stabilizing agent in aqueous solution of $HAuCl_4$ we were able to control the size and shape of nanoparticles by changing the synthesis parameters.

Next, in **Chapter 4** we selected the smaller spherical shaped AuNPs previously synthesized, denoted AuNPs@gelatin, to investigate their interaction with Osteoblast cells. Standard citrate coated AuNPs with similar shape and size were used as control. The results revealed the increased osteoblasts proliferation and differentiation in the presence of higher AuNPs@gelatin concentrations.

Chapter 5 describes the fabrication of a new pH-responsive chemotherapeutic nano-system based on AuNPs@gelatin loaded with conventional chemotherapeutic drug Doxorubicin. We tested the *in vitro* efficiency of obtained DOX-AuNPs@gelatin complex on the MCF-7 breast cancer cell line using dark field scattering imaging, fluorescence microscopy, fluorescence-lifetime imaging microscopy (FLIM), SERS spectroscopy and MTT assay.

In the last chapter of my thesis, **Chapter 6**, are summarized the conclusions and perspectives of my studies.

Part III presents the Annexes of my thesis.

Keywords: *gold nanoparticles, gelatin, biosynthesis, cancer therapy, Doxorubicin, cells culture, surface plasmons, fluorescence microscopy, FLIM, SERS*

Part I
Introduction and Review of related literature

Chapter 1
Literature Review

1.1. Introduction

Taking into account the AuNPs properties, ease of synthesis and functionalization, they are currently considered as building blocks for many nanostructured materials and devices [1]. It is also possible to design complex, sophisticated nanomaterials combing different organic and inorganic materials which will act in a synergistic manner in one nano-system that will be able to pass all the barriers from the human body [2] to repair damaged tissues and restore its function. These new materials gave rise to a new domain – nanomedicine – focused primarily to develop novel nano-systems that allow simultaneous diagnostic, imaging and therapy [3], especially useful for personalized treatment of cancer [4].

1.2. Synthesis methods of gold nanoparticles

The most popular method for the synthesis of spherical AuNPs is the classical Turkevich method which involves the reduction of $HAuCl_4$ by sodium citrate in aqueous solution at boiling temperature. Depending on the desired application, different sized nanoparticles with diameters ranging from 10 to 150 nm can be obtained simply by varying the ratio of the two reactants.

Other methods for the synthesis of AuNPs are the Brust – Schiffrin method used to produce very small AuNPs in organic liquids or the use of capping agents strategy which are able to control the growth rates of various facets of seeds to obtain anisotropic metal nanoparticles such as rods, wires, triangles, stars or flowers.

Although these methods provide high quality nanoparticles it makes use of some chemical agents (e.g. sodium citrate or sodium borohydride) known for potential biological risks, to provide only limited stability to AuNPs in biological media and that further requires their purification and biocompatibilization in order to be used in biological/biomedical applications.

However, the "green chemistry" protocols gained more and more interest in the NPs synthesis field due to the eco-friendly materials used. For example, synthesis protocols employing bacteria, fungi or yeasts as well as amino acids, vitamins, biopolymers, live plants or plant extract are involved not only to reduce metallic ions into well-defined shape and size NPs but subsequently to cover and protect the formed NPs while confer them a functionalized surface [5], in only a single step. Therefore, AuNPs biosynthesis maximize the efficiency and safety of reactions while minimize the environmental risks.

1.3. Gold nanoparticles properties

In the range of nanometer scale due to the large surface area or quantum size effect, physical and chemical properties of materials change drastically resulting in unique properties. These distinctive characteristics appear from the collective oscillation of free electrons under light excitation, known as localized surface plasmon resonance (LSPR). The LSPR band of AuNPs is highly dependent on the size, surface chemistry and local environment around AuNPs being thus a useful probe to monitor the nanoparticles interaction with biological samples. These unique features can be tuned precisely to interfere specifically with organic matter in order to facilitate its application in biomedical field.

Another important property of AuNPs is the enhanced electromagnetic field generated around their surface. This electromagnetic field can enhance the fluorescence of a molecule in the proximity of a nanoparticles and the Raman signal of molecules from the metallic surface.

1.4. Biomedical applications of gold nanoparticles

Given the versatility of AuNPs which provide complex materials, these have huge applications in nanomedicine such as targeted delivery of drugs and gene, genomics, biosensoristics, biodetection or optical bioimaging.

1.4.1. Gold nanoparticles in biosensing applications

The simplest sensing method based on nanotechnology is colorimetric detection which is based on the interaction/binding between functionalized AuNPs and analytes that induce the aggregation of AuNPs and subsequent visual color change from red to blue.

Biosensing based on LSPR shift is a method that relies on the change in the intensity and spectral shift of LSPR band induced by a variation in the local environment of AuNPs following biospecific interactions [6]. It is less sensitive than the aggregation assays, and given that any molecule can induce a shift in LSPR band of AuNPs, this method is exclusively suitable for detection of known analytes and only when AuNPs are functionalized with molecular recognition elements such as antibodies.

For the detection and identification of unknown samples, Raman spectroscopy is the method of choice because it is a highly specific technique able to identify molecular species based on their unique vibrational Raman fingerprint. The Raman signal can be drastically amplified when the analytes are adsorbed on metallic surfaces, known as surface enhanced Raman scattering. For efficient biosensing applications is therefore essential the SERS substrate. In solution, the Au nanospheres aggregation or anisotropic AuNPs cause the hot-spots formation between interconnected nanoparticles which substantially enhance the Raman signal. Equally important as AuNPs shape is the functionalization and biocompatibility of sensor that should permit the adsorption of analytes for a highly efficient, stable and reproducible SERS signal.

1.4.2. Gold nanoparticles in imaging applications

The versatile optical and electronic properties of AuNPs have enabled cell imaging with a variety of techniques, including dark-field light scattering, optical coherence tomography (OCT), computed tomography (CT), atomic force microscopy (AFM), fluorescence, transmission and scanning electron microscopy (TEM, SEM) as well as SERS spectroscopy. Some of these techniques currently used even allow single cell imaging.

1.4.3. Gold nanoparticles in delivery applications

Depending on surface functionalization, type of drug and desired application, AuNPs can be easily loaded with a single or multiple drugs or other molecules through either non-covalent interactions or covalent conjugation. Loading of drugs onto AuNPs improve its stability and biodistribution in biological media since the drugs are protected in the carrier, confer them a longer life in biological systems and the possibility to be delivered by either targeted or passive ways to the site of action.

AuNPs allow a huge loading of drugs due to large surface area and versatile surface chemistry. Moreover, enhanced activity of drugs delivered by AuNPs makes possible the reduction of drug dose administered and subsequently its undesirable side effects.

1.4.4. Other biomedical applications of gold nanoparticles

In photodynamic therapy (PDT) AuNPs are widely employed as carrier of photosensitizing agents to the target area. There, the excited photosensitizer can produce a highly reactive state of oxygen known as singlet oxygen that kills nearby cells.

AuNPs are also frequently used in photothermal therapy (PTT) due to its unique interaction with laser irradiation. AuNPs located inside or around the target cells, upon laser irradiation absorb photon energy which is converted into heat energy and induce an increase of the local temperature around AuNPs and therefore the damage of these cells [7].

In addition, AuNPs can be applied simply as therapeutic or effective antibacterial agents.

1.5. Gold nanoparticles for cancer detection, imaging and treatment

In order to achieve maximal results in cancer detection and treatment with minimal side effects is crucial that therapeutic agents to reach at the tumor site and inside the malignant cells. Conventional medicine, typically involves chemotherapy to treat cancer, but unfortunately chemotherapeutic agents are not specific to cancer cells, therefore destroys malignant and normal cells as well, are highly toxic and have many undesired side effects [8]. Nanomedicine, on the other hand, makes use of nanostructured materials able to carry and release chemotherapeutic agents specifically only at the cancerous tissue.

In this section, we briefly review the most important cancer treatment approach based on AuNPs and doxorubicin drug – a widely used chemotherapeutic agent with proved effects against leukemia, lymphomas, ovaries, breast cancer, and many solid tumors.

Part II

Research Results and Discussions

Chapter 2

Gelatin-nanogold bioconjugates: formation, stability and decoration with some therapeutic functionalities

2.1. Gold nanoparticles functionalization

2.1.1. Characterization of gelatin@AuNPs bioconjugates

The formation of gelatin@AuNPs bioconjugates were realized in one step process simply by mixing 100 µl of gelatin solution – at different concentration values – with 1 ml of colloidal gold solution. Subsequently, we denoted as 0.03gelatin@AuNPs and 10gelatin@AuNPs the bioconjugates prepared in the presence of gelatin concentration of 0.03 and 10 mg/ml, respectively. The samples were centrifuged for 10 min at 12000 RPM to remove the free gelatin and then were redispersed in ultrapure water.

The position and shape of LSPR band were analyzed to infer the binding of gelatin layer on the surface of citrate-synthesized AuNPs and conclude about the stability of gelatin@AuNPs bioconjugates.

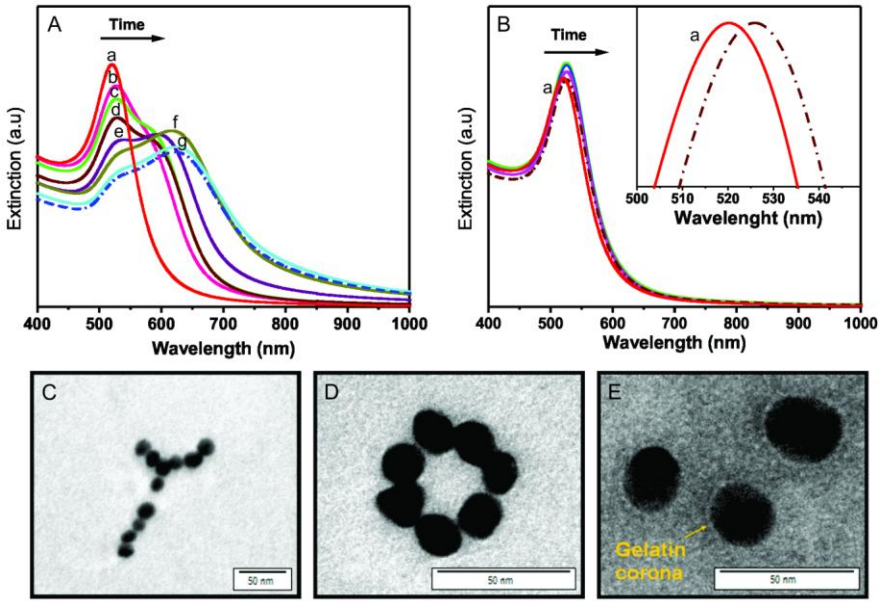

Figure 2.1. A. Time evolution of 0.03gelatin@AuNPs and **B.** 10gelatin@AuNPs plasmonic spectra, respectively. **C.-D.** TEM pictures of 0.03gelatin@AuNPs and **E.** 10gelatin@AuNPs, showing short chains and necklace rings structures, respectively individual gelatin coated AuNPs

Firstly, we compare the spectra of two representative samples prepared at low (Figure 2.1.A) and high (Figure 2.1.B) gelatin concentrations (0.03gelatin@AuNPs and 10gelatin@AuNPs samples). We use for reference the LSPR band of citrate-coated AuNPs (Figure 2.1.A spectrum a) located at 520 nm typical for spherical nanoparticles of 18±2 nm diameter as provided by TEM measurements and hydrodynamic diameter of 25 nm. The presence of citrate anions layer at the surface of reference AuNPs is confirmed by ζ-potential of -31.5 mV.

Figure 2.1.A shows a selection of LSPR spectra recorded successively during the stabilization process of 0.03gelatin@AuNPs sample, which expose two bands and reveals a controlled aggregation process. The phenomenon of aggregation by which small aggregates are formed in solution on the expense of free AuNPs conduce to formation of small ensembles of nanoparticles, as TEM pictures in Figure 2.1.C-D confirm.

Similarly, we analyze the modifications in LSPR spectra recorded at different time intervals during the stabilization process of second sample, refereed as 10gelatin@AuNPs (Figure 2.1.B). The first observation is that the stabilization process is fast, lasting no more than 15 minutes, opposite to about two days in the case of 0.03gelatin@AuNPs. The only modification is a red shift of 5 nm (spectra and inset in Figure 2.1.B) from 520 nm to 525 nm with an almost no modification in the band shape, clearly indicating the behavior of individual nanoparticles in solution. Corroborating evidences from TEM picture (Figure 2.1.E), DLS (increase of the hydrodynamic diameter to 65±5 nm) and ζ-potential measurements (increase to +6.44±2.4 mV) is confirmed the presence of gelatin layer onto AuNPs surface.

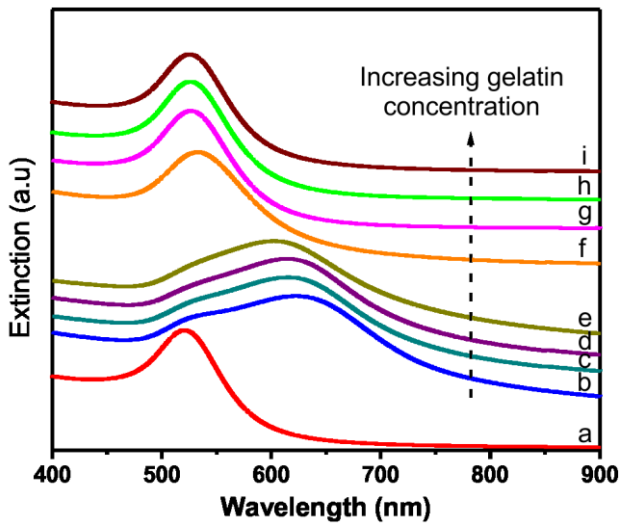

Figure 2.2. LSPR spectra of reference sample (spectrum a) and gelatin@AuNPs bioconjugates formed in presence of different gelatin concentrations: b) 0.03 mg/ml, c) 0.05 mg/ml d) 0.07 mg/ml e) 0.1 mg/ml f) 0.3 mg/ml g) 1 mg/ml h) 5 mg/ml and i) 10 mg/ml

We have also investigated the evolution of LSPR spectra for several examples of samples prepared with gelatin concentrations ranging from 0.03 to 10 mg/ml. All samples exhibit stable LSPR spectra (Figure 2.2) after shorter or longer incubation time, consistent with mixtures of

isolated and small aggregates those ratios can be controlled by gelatin concentration. The corresponding DLS measurements provide additional information, confirming the presence of aggregates of large hydrodynamic diameter at very low gelatin concentration that decrease as gelatin concentration increases. Accordingly, the surface charge of bioconjugates varies with gelatin concentrations in the range 0.03 - 10 mg/ml until it reaches a steady-state positive value of +6.44±2.4 mV for 10 mg/ml.

2.1.2. FT-IR analysis of gelatin-AuNPs interaction

The polymeric chain of gelatin exhibits both amine, carboxyl and amide functional groups, gelatin peptide are positively charged at physiological pH and adsorb electrostatically on negatively charged citrate-capped AuNPs.

The details of molecular structure and specific interaction of gelatin with AuNPs is further characterized by FT-IR spectroscopy (Figure 2.3)

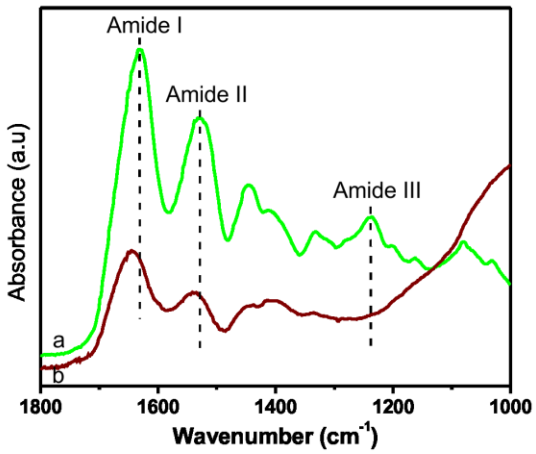

Figure 2.3. FT-IR spectra of a) gelatin and b) 10gelatin@AuNPs bioconjugates

The amide I band, sensitive to changes in the gelatin chain conformation [9] shift from 1632 cm^{-1} to 1650 cm^{-1}, suggesting that the secondary structure of gelatin was changed from β-antiparallel sheets to α-helix, after conjugation with AuNPs.

Moreover, the amide III band observed in the case of pure gelatin (mainly due to C–N stretching vibration), disappears in the case of gelatin bind to the surface of AuNPs. This behavior indicates the blocking of the C–N stretching vibration due to the coordination of $–NH_2$ functional group from amide group to the gold nanoparticles surface.

These results suggest that the amide and carboxylic groups can be especially active sites for the coordination with surface of AuNPs, clearly indicating that the nanoparticles were indeed conjugated with the biopolymer.

2.2. Gelatin@AuNPs bioconjugates as SERS active substrates

Two examples of gelatin@AuNPs bioconjugates (individual and aggregated) were tested as SERS substrates in solution of $3.6 \cdot 10^{-6}$ M RB (Rose Bengal) concentration under laser excitation lines at 532 nm and 633 nm. No Raman signal could be recorded from solution of identical RB concentration ($3.6 \cdot 10^{-6}$ M) prepared without bioconjugates (Figure 2.4 spectrum a) and, for reference, we collected a normal Raman spectrum from a solution of much higher concentration (10^{-2} M) under 633 nm laser excitation line (Figure 2.4 spectrum b).

The SERS measurements reveal the presence of RB molecules in bioconjugates. Specifically, for RB-incubated individual gelatin@AuNPs (RB-10gelatin@AuNPs), the 532 nm laser line which is simultaneously resonant with LSPR band of AuNPs at 525 nm and the electronic absorption band of RB at 548 nm, enables the record of a surface-enhanced resonance Raman scattering (SERRS) spectrum (Figure 2.4 spectrum e) [10]. The RRS contribution is clearly reveled (Figure 2.4 spectrum e) by the occurrence of two strong bands located at 1619 cm^{-1} and 1496 cm^{-1} assignable to molecular ring vibrations which represent the hallmarks of chromophore excitation. This result suggest that part of RB molecules are attached to polymer not direct to metal surface to prevent fluorescence quenching, but not too far from metal to compromise the SERS activity. In the case of aggregated bioconjugates (RB-0.03gelatin@AuNPs) the main LSPR band at 622 nm is located far from the excitation laser line at 532 nm. As result only small fraction of individual bioconjugates existing in solution in presence of aggregated bioconjugates are SERS-active, which makes that the recorded fluorescence completely overlaps the SERRS signal of RB reporter molecule.

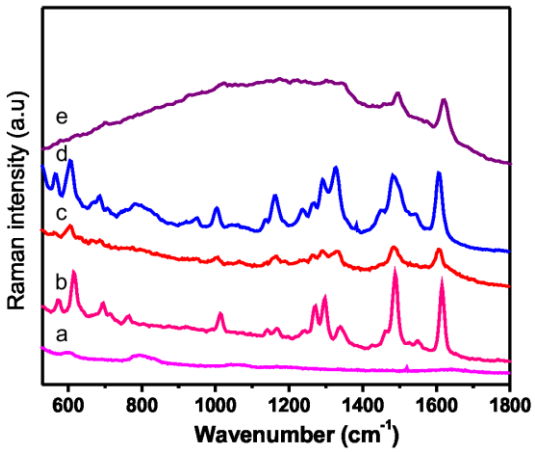

Figure 2.4. Reference Raman spectrum of free RB of a) $3.6*10^{-6}$ M and b)10^{-2} M in solution recorded at 633 nm; SERS spectra of c) RB-individual 10gelatin@AuNPs, d) RB-interconnected 0.03gelatin@AuNPs recorded at 633 nm and e)RB-individual 10gelatin@AuNPs recorded at 532

Next we analyze the SERS spectra recorded from the samples (0.03gelatin@AuNPs and 10gelatin@AuNPs) under excitation at 633 nm laser line. As the electronic absorption band of RB is located at 548 nm no resonant Raman effects can contribute to SERS. In the case of

0.03gelatin@AuNPs sample the laser line is resonant with LSPR band of small aggregates at 633 nm which allows recording a very good SERS signal (Figure 2.4 spectrum d). We assume that a significant contribution of SERS originates from the number of hot-spots occurring between small gaps induced by aggregation [11]. On the contrary, in the case of 10gelatin@AuNPs sample, the laser line is out of resonance of bioconjugates which makes the SERS signal extremely weak (Figure 2.4 spectrum c).

2.3. Gelatin@AuNPs bioconjugates as substrates for loading of FLT3 inhibitors

We propose a new method to deliver inhibitors of Fms-like tyrosine kinase 3 (FLT3 inhibitors) to AML cells by using individual AuNPs protected in a gelatin envelope as a drug carrier, complex able to embed high drug concentrations and transport it in a controlled manner to the malignant cell, thus reducing the dosage in healthy tissues and reducing severe, life threatening side effects. In our study, we have selected four different FLT3 inhibitors, namely midostaurin (MDS), sorafenib (SRF), lestaurtinib (LST) and quizartinib (QZR) to design a novel AuNPs-drug system for AML therapy.

Four sets of UV-Vis spectra corresponding to the four different FLT3 inhibitors (MDS, SRF, LST and QZR) conjugated to gelatin@AuNPs are presented in Figure 2.5 A, B, C and D, respectively. In each case, the UV-Vis spectrum of gelatin@AuNPs (without drug) and the free drug is presented for reference.

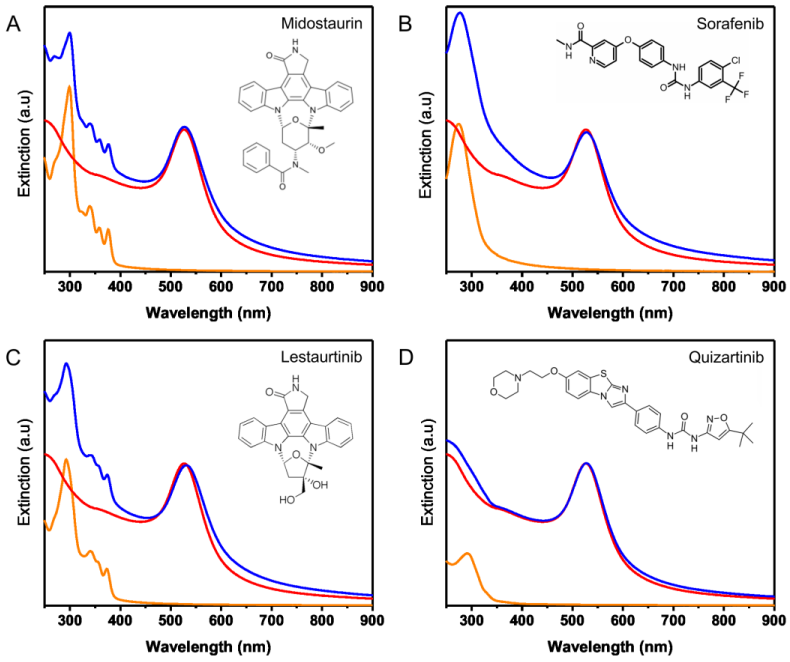

Figure 2.5. Loading of FLT3 inhibitors (orange spectrum) onto gelatin@AuNPs (red spectrum) Blue spectra represents: **A.** gelatin@AuNPs-MDS, **B.** gelatin@AuNPs-SRF, **C.** gelatin@AuNPs-LST and **D.** gelatin@AuNPs-QZR. Insets presents chemical structures of the FLT3 inhibitors

The purified gelatin@AuNPs presents a characteristic LSPR plasmonic signature which has a maximum centered at 526 nm (red spectrum in each quadrant of the Figure 2.5). In all cases, after incubation of gelatin@AuNPs with FLT3 inhibitors, the complexes present red-shifted LSPR band together with the drug signature in the UV region, which can be considered as the first proof of interaction between FLT3 inhibitors and AuNPs. The shape similarity of the plasmonic band indicates that the formed complexes are individually dispersed in the solution and represent a sign of stability.

The loading of the FLT3 inhibitors onto gelatin@AuNPs is also sustained by the zeta potential and dynamic light scattering (DLS) measurements. After purification, unloaded gelatin@AuNPs bears a positive charge of +22.5±0.4 mV that comes from the gelatin layer from the AuNPs surface. Following interaction with the drugs, the zeta potential of nanoparticles increases up to +30.4±0.8 mV for gelatin@AuNPs-LST and even +32.4±0.4 mV for gelatin@AuNPs-QZR, confirming the adsorption of the drugs onto particles surface. Additionally, a ζ-potential value higher than +30 mV represents a major sign of complex stability. DLS characterization of purified gelatin@AuNPs before and after drug interaction reveals the increase of hydrodynamic diameter after loading of the drugs, confirming the ability of the gelatin layer from AuNPs surface to incorporate a high amount of drug.

To perform as efficient FLT3 inhibitor nano-systems in *in vitro* and *in vivo* applications, an open question still remains the stability of the drug loaded gelatin@AuNPs in biological conditions where it can become prone to aggregation. In this regard, the long term stability of our different drug complexes was proved by measuring the plasmonic response of gelatin@AuNPs after one week storage in PBS solution

Chapter 3

One-pot, gelatin-assisted synthesis of gold nanoparticles

3.1. Gold nanoparticles biosynthesis

3.1.1. Tuning size and shape of AuNPs as function of gelatin concentration

The synthesis of AuNPs was realized by simply mixing different concentrations of gelatin solution with 3 mM $HAuCl_4$ solution in a volume ratio of 1:1 and incubated for 6 h at 80 °C. We monitored the formation of AuNPs using both the UV-Visible absorption spectroscopy and TEM images of as-synthesized nanoparticles deposited on TEM grids. In the first series of experiments we examined the formation of AuNPs as result of mixing identical amount of tetrachloroauric acid ($HAuCl_4$) solution with solutions of various concentrations of gelatin. Figure 3.1.A shows typical examples of LSPR spectra recorded from 5 colloidal solutions of AuNPs resulted after

incubation of precursor solutions with increasing gelatin concentrations: 0.5%, 0.62%, 0.75%, 0.87% and 1%. Noteworthy, all measurements were performed after 6 h of incubation at 80 °C in each case, when formation of nanoparticles was stopped by cooling down the solutions at room temperature.

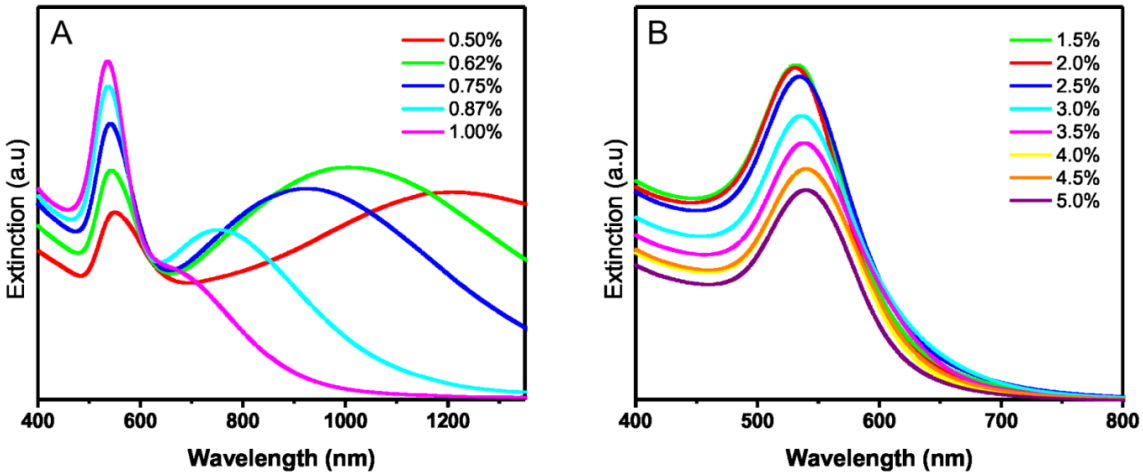

Figure 3.1. UV-Vis-NIR spectra of as-synthesized AuNPs with **A.** low gelatin concentrations and **B.** high gelatin concentrations

In the range of above concentrations, spectra exhibit at least two extinction bands which evolve as function of gelatin concentration. Specifically, the position of the first band located at about 530 nm remains relatively stable in time and their intensity increases steadily while the second band gradually shifts from NIR (~1300 nm) to visible (~650 nm) becoming narrower as gelatin concentration increases. According to literature the second band can be assigned to in-plane dipole resonance while the first band to out of plan dipole resonance of triangular AuNPs which overlaps the plasmon resonance of spherical AuNPs [12]. TEM images confirm the prevalence of triangular nanoparticles (~69%) against of spherical nanoparticles (~31%) at lowest gelatin concentration and the prevalence of spherical nanoparticles (~78%) against highly polydisperse nanotriangles (~22%) at higher gelatin concentration. The gradual shift of in-plane dipole resonance of nanotriangles from NIR to visible with increasing gelatin concentration is corroborated with a decrease of nanotriangles edge from 237±17 nm to 52.5±21 nm, as resulted from TEM analysis.

In contrast, in the second series of experiments performed at increasing gelatin concentrations of 1.5%, 2%, 2.5%, 3%, 3.5%, 4%, 4.5% and 5%, the LSPR band in NIR disappears completely and the remaining band in visible steadily shifts from 530 nm to 540 nm. This red-shift accompanied by a progressive decrease in band intensity, denotes an increase in nanoparticles size together with decrease in the concentration of formed nanoparticles (Figure 3.1.B). Again, TEM images confirm the formation of spherical AuNPs of average diameter from 18±3.5 nm to 57±10 nm.

3.2. Gold nanoparticles growth and characterization

3.2.1. The effect of gelatin concentration on the AuNPs growth and morphology

We also monitored the formation of AuNPs at 80 °C as function of incubation time by measuring LSPR spectra of solutions at varying times of synthesis process for two representative cases, i.e. the case of high (1.5%) and low gelatin concentration (0.5%), respectively. In the first case, the LSPR band and corresponding change in solution color occurred only after one hour of incubation (Figure 3.2.A). The LSPR band emerges at 540 nm and increases in intensity simultaneously with a progressive blue shift to 530 nm after almost 6 h.

The blue-shift of LSPR band can be partially explained by modification of dielectric environment of AuNPs which can be due to the dissociation of small gelatin clusters occurred when the particles growth is sustained by a diffusion-controlled Ostwald-ripening.

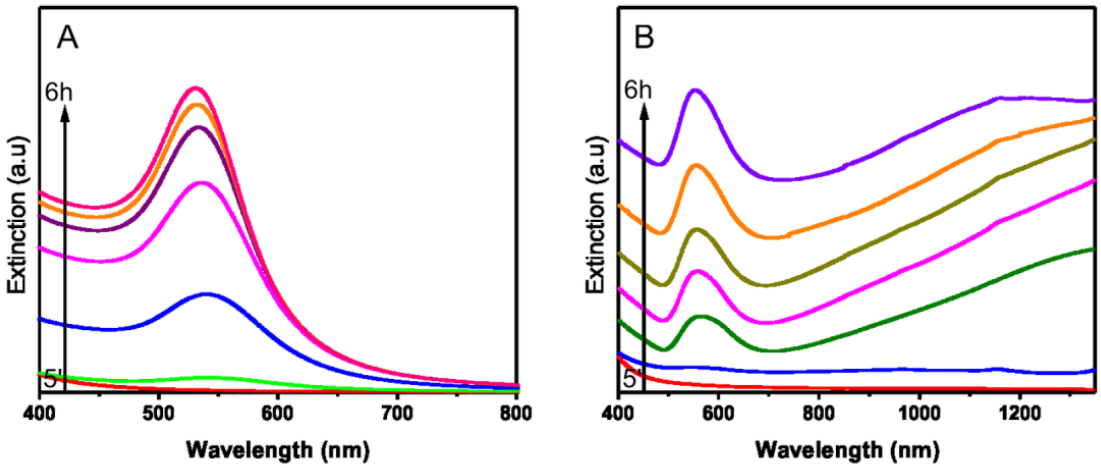

Figure 3.2. The intensity and spectral position evolution of LSPR band associated with gelatin-assisted AuNPs synthesis at **A.** 1.5% gelatin concentration and **B.** 0.5% gelatin concentration (Recorded spectra were translated for a better visualization in Figure B)

As regards the second case, the incubation of gold ions with low gelatin concentration (0.5%) at 80 °C is associated with a more complex evolution of LSPR spectrum. Interestingly, LSPR band featuring the formation of AuNPs of triangular shapes emerges at 1158 nm and, as the synthesis continues, this band evolves in time toward 1200 nm after 6 h (Figure 3.6.B), 2indicating the growth of the nanotriangles [13]. The first LSPR band at 553 nm corresponding to composed out-of-plane dipole resonance of triangular nanoplates and plasmon resonance of spherical AuNPs has a similar behavior with that previously discussed in the case of nanospheres synthesis. It is worth mentioning that in both cases the synthesis reaction was stopped and the shape and size of formed nanoparticles remained unchanged after cooling down the colloidal solution at room temperature.

3.2.2. The effect of synthesis temperature on the nanoparticles growth

Previously, we have focused on the formation of gelatin-coated AuNPs at 80 °C but gelatin in solution is susceptible to degradation at elevated temperature. Therefore, the formation of AuNPs at lower temperatures corroborated with viscosity data is presented here.

Figure 3.3.A shows the sequence of LSPR spectra recorded in the first 6 h from three identical solutions incubated at temperatures of 40 °C, 60 °C and 80 °C. It is clear that at temperature just above and at any temperature below the melting point of gelatin the synthesis of AuNPs is not feasible.

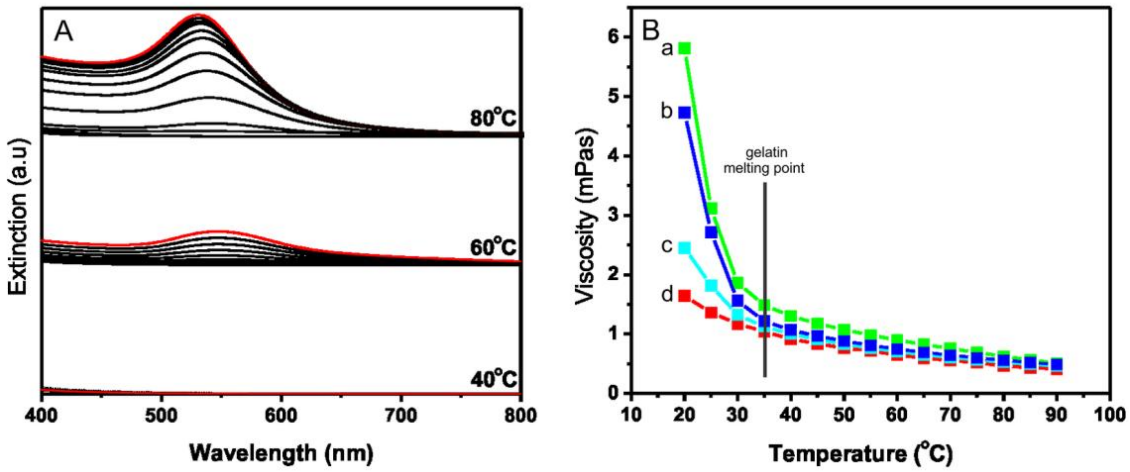

Figure 3.3. A. The time evolution of the LSPR band intensity recorded during AuNPs synthesis at 40 °C, 60 °C and 80 °C; **B.** Viscosity vs. temperature dependence for a) pure gelatin solution before thermal treatment; pure gelatin solution after 6 h of heating at b) 60 °C and c) 80 °C, respectively, and d) colloidal suspension of gelatin-coated AuNPs as synthesized at 80 °C

It is not surprising since gelatin exhibits reduced viscosity and random coil conformation above the gel melting point (~35 °C) and an increased viscosity with triple helical regions below this point (Figure 3.3.B) [14]. Increased viscosity slows the synthesis considerably due to reduced transfer of electrons between the amine groups of gelatin and gold ions while a reduced gelatin viscosity facilitates an increased synthesis rate.

The sample incubated at 80 °C shows LSPR band at 530 nm while the sample incubated at 60 °C present similar LSPR band red-shifted at 547 nm assigned to spherical AuNPs. The intensity of LSPR band in Figure 3.3 demonstrates that synthesis carried out at 80 °C is much faster and higher nanoparticles concentration is achieved. Explicitly, a higher temperature imposes a fast nucleation step which subsequently leads to the formation of larger number of particles of relatively smaller size, confirmed by TEM images (Figure 3.4).

Additionally, above 60 °C in gelatin biopolymer is noticed a thermal degradation and dissociation of hydrogen bonds which impose the formation of gelatin monomers [15]. Gelatin monomers expose more hydroxyl groups which are known as efficient reducing agents for gold ions.

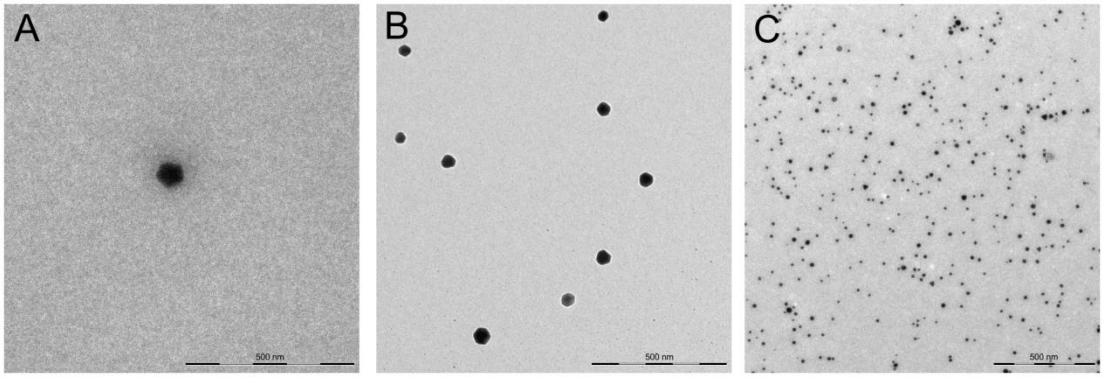

Figure 3.4. TEM images of AuNPs bio-synthesized at **A.** 40 °C, **B.** 60 °C and **C.** 80 °C. Scale bars indicate 500 nm

Therefore, the faster reduction of gold ions in the presence of degraded gelatin is enabled [16]. Furthermore, the gelatin incubation at higher temperatures promotes an increase in the degree of degradation which can be seen by comparing the viscosity curves of a gelatin solution before (Figure 3.3 curve a) and after the thermal treatment for 6 h at 60 °C and 80 °C, respectively (Figure 3.3 curves b and c). These modifications could also influence the refractive index of gelatin, which have an impact on the LSPR band shift.

The viscosity of AuNPs biosynthesized by gelatin biopolymer also slowly decreases while the temperature increases, due to viscosity change of gelatin protecting layer from their surface (Figure 3.3 curve d).

3.3. The stability of the gelatin coated gold nanoparticles

3.3.1. AuNPs stability in simulated physiological media and cellular medium

For next studies we selected from the large variety of nanoparticles obtained, the AuNPs synthesized with 1.5% gelatin concentration (referred here as AuNPs@gelatin) since they are the smallest spheres obtained and the most monodisperse nanoparticles, with a size of 18±3.5 nm as evidenced by TEM image and corresponding histograms.

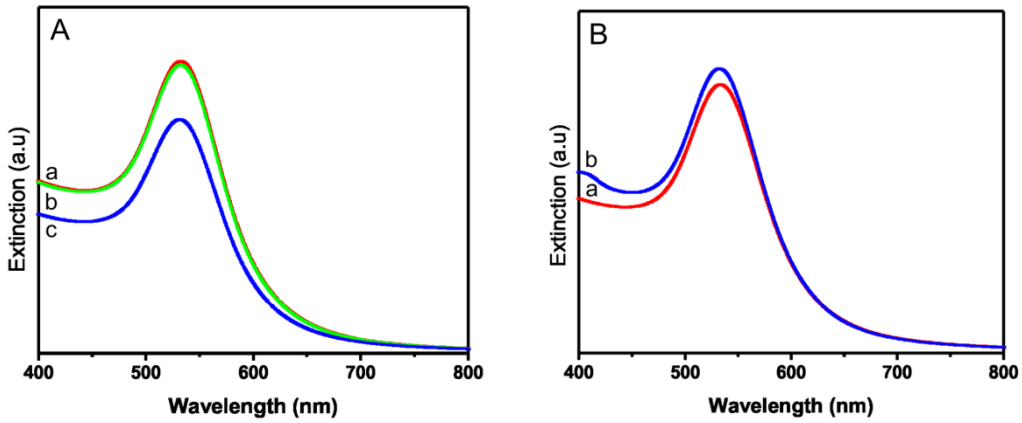

Figure 3.5. A. LSPR spectra of gelatin synthesized/stabilized AuNPs a) after purification b) at physiological temperature of 37 °C and c) in 0.9% NaCl solution.
B. AuNPs@gelatin extinction spectra recorded in a) ultrapure water and b) cellular medium

In view of their use in biomedical applications, the stability of AuNPs was firstly proved by monitoring the evolution of LSPR spectra in simulated physiological conditions (i.e. 0.9% NaCl solution and 37 °C) and in DMEM/F12 cellular medium at physiological temperature. No sign of aggregation induced in LSPR band was observed. These results demonstrate that gelatin act as an efficient capping/protecting agent for AuNPs and additionally offer the guarantee that AuNPs@gelatin are perfectly stable both in simulated and cellular medium at physiological temperature (Figure 3.5).

Chapter 4

Biocompatibility and biological effects of gelatin coated gold nanoparticles on Osteoblast cells

4.1. Internalization of gold nanoparticles into osteoblast cells

Figure 4.1 shows the dark-field images of osteoblast (OBL) cells treated with AuNPs@gelatin (Figure 4.1.B) together with control cells treated with citrate coated AuNPs (Figure 4.1.C) and untreated cells (Figure 4.1.A). Some bluish dots are visible in control untreated cells due to the characteristic scattering of the intrinsic cellular organelles [17] while a strong scattering appears from treated cells which shows inside some yellowish-orange spots that obviously confirm the AuNPs@gelatin and AuNPs@citrate uptake by OBL.

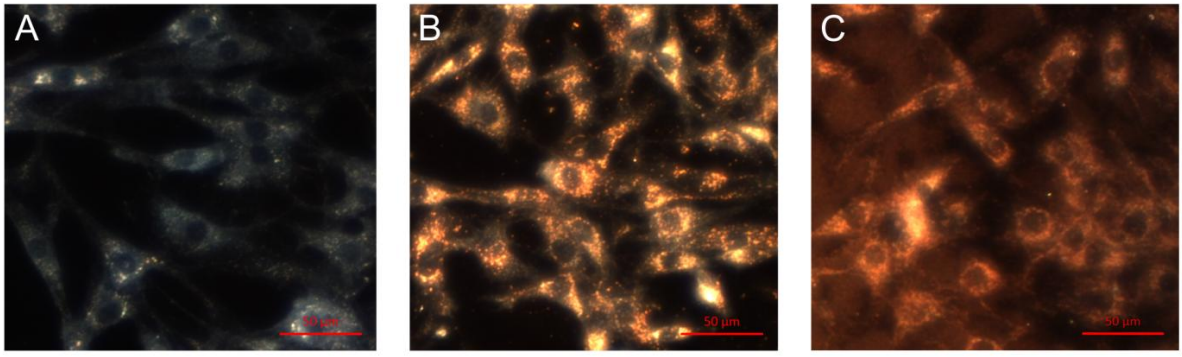

Figure 4.1. Dark-field images of **A.** untreated control OBL cells and, **B.** AuNPs@gelatin and **C.** AuNPs@citrate treated OBL cells. The scale bars indicate 50 µm.

A significant difference between the uptake of negatively charged AuNPs@citrate (-31,5±1.8 mV) and positively charged AuNPs@gelatin (+27±1.2 mV) is observed in dark-field microscopy, most likely due to the electrostatic interaction of nanoparticles with outer cell membrane which is overall negatively charged. Additionally, in the case of cells treated with AuNPs@citrate, contrary to AuNPs@gelatin treated cells, a high amount of aggregated AuNPs@citrate can be observed on the substrate, suggesting a low stability in the absence of a protecting coating at their surface. Rayleigh scattering spectra collected from inside the cells treated with the same concentration of AuNPs@gelatin and AuNPs@citrate also confirm this

observation, proving the stability of AuNPs@gelatin, which present their typical spectra while AuNPs@citrate shows a broad, red-shifted spectrum characteristic to aggregated nanoparticles.

For a more accurate investigation of AuNPs internalization we employed DIC microscopy, since it enables optical sectioning of a cell with a high precision providing a complex visualization of both cellular organelles and internalized AuNPs.

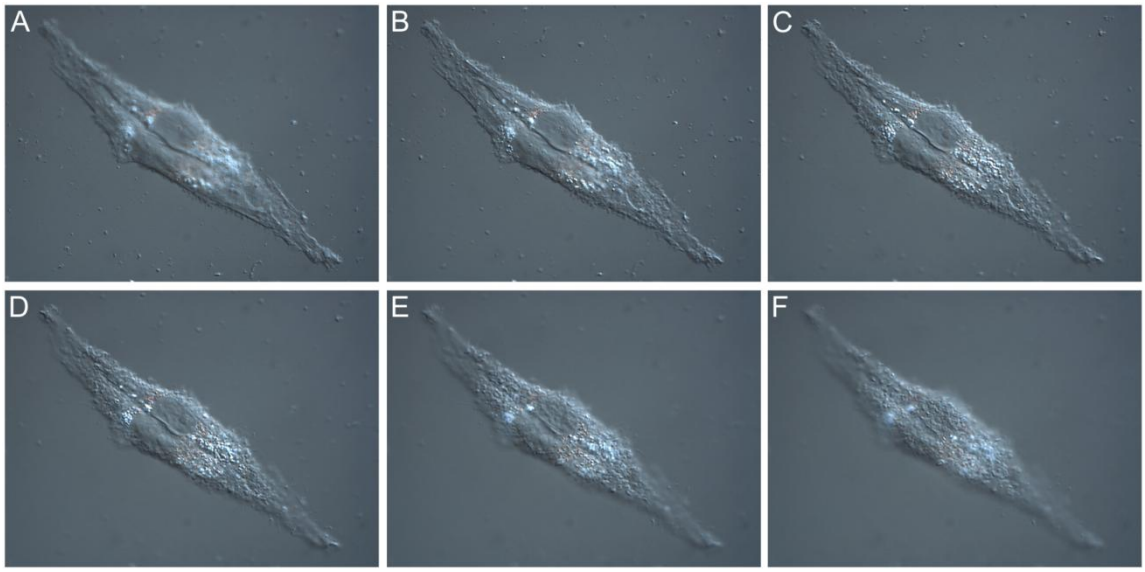

Figure 4.2. DIC images of OBL cells treated with AuNPs@gelatin for 24 h at different depths (A) - (F) Z=3-8 µm

The imaging of OBL cells treated with AuNPs@gelatin by focalizing at different planes of cell in the Z direction (Figure 4.2) depicts the AuNPs localization within the whole cytoplasmic region in the entire depth of the cells. DIC images prove the dark-field result, showing AuNPs localization exclusively outside of nuclei.

4.2. Gold nanoparticles effect on osteoblast cells proliferation

Next, we investigated the *in vitro* biocompatibility/cytotoxicity of AuNPs@gelatin, AuNPs@citrate, gelatin biopolymer using MTT cytotoxicity assay on osteoblast cells. The cells were exposed to different AuNPs@gelatin, AuNPs@citrate, gelatin biopolymer concentrations (1-100 µg/ml) for 24, 48 and 72 h, respectively.

As can be seen in Figure 4.3, OBL cells present excellent viability, AuNPs@gelatin shows no toxic effects even at high nanoparticles concentration and do not inhibit the proliferation. Instead, cells growth and proliferation present higher increase rates in samples treated with AuNPs@gelatin compared to cells treated with AuNPs@citrate or gelatin alone reported to untreated control samples. The osteoblasts proliferation was progressively promoted in presence of higher nanoparticles concentrations (50-100 µg/ml) even at long-time exposure (72 h).

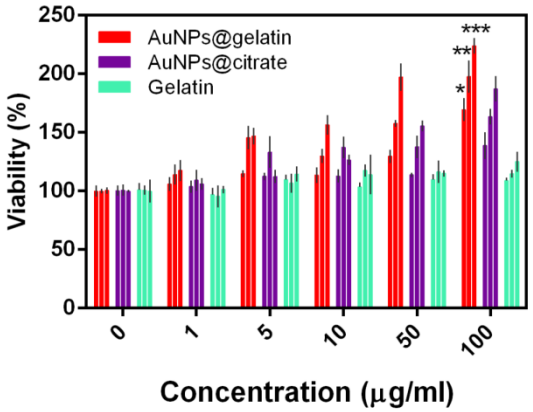

Figure 4.3. Viability of OBL cells treated with different concentrations of AuNPs@gelatin, AuNPs@citrate and Gelatin biopolymer for (*) 24, (**) 48, and (***) 72 h investigated by MTT assay. Error bars represents the standard deviation from 3 replicated experiments.

The presence of AuNPs stimulates the cells growth and proliferation, by quenching the free radicals formed during cellular growth and acting as antioxidant agents. Moreover, we assume that the cells treated with AuNPs@gelatin show an increased proliferation rate due to the synergistic effect between AuNPs and gelatin layer which covers the metallic surface.

4.3. Gold nanoparticles effect on osteoblast cells differentiation

AuNPs@gelatin treated OBL cells showed outstanding cell proliferation and more interestingly, a first sign of differentiation with bone nodules formation which reveal their osteogenic effect (Figure 4.4.A).

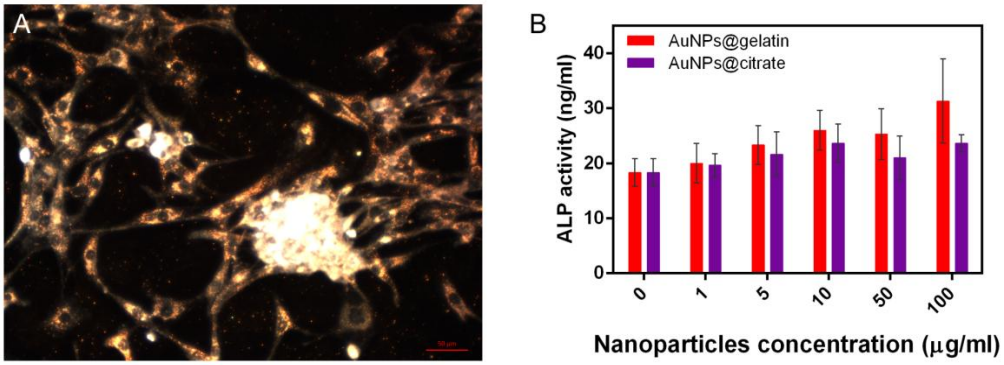

Figure 4.4. A. Dark-field image of OBL cells treated with AuNPs@gelatin showing a first sign of cells differentiation with bone nodules formation. The scale bar shows 50 µm.
B. Dose-dependent effects of AuNPs@gelatin and AuNP@citrate on the ALP activity of OBL cells after 72 h treatment. Error bars - standard deviation from a triplicate experiment.

Osteoblast differentiation is an essential aspect of bone formation and remodeling, therefore, the effect of AuNPs@gelatin on OBL differentiation was investigated by alkaline phosphate (ALP) activity assay, since the appearance of ALP activity is an early phenotypic marker of osteoblast differentiation [18]. The ALP activity shown by OBL cells treated for 72 h

with AuNPs@gelatin is significantly higher than AuNPs@citrate treated cells, especially at higher concentrations, i.e. 50, 100 μg/ml. As in the case of cells proliferation, the cells treatment with gelatin biopolymer (100 μg/ml) has a lower effect on ALP activity, compared with AuNPs@gelatin treatment in the same concentration.

Alkaline phosphatase protein expression was also investigated by immunocytochemical staining of OBL cells treated with 100 μg/ml AuNPs@gelatin. Triple coloration staining (Figure 4.5) allows an accurate observation of OBL cells adhesion and spreading process marked by actin-F fibers organization (stained red with phalloidin TRITC), cells nuclei (stained blue with DAPI) and ALP expression highlighted by green FITC staining. These results are consistent with the MTT results and further confirm the better proliferation and osteoblast differentiation in the presence of higher AuNPs@gelatin concentrations.

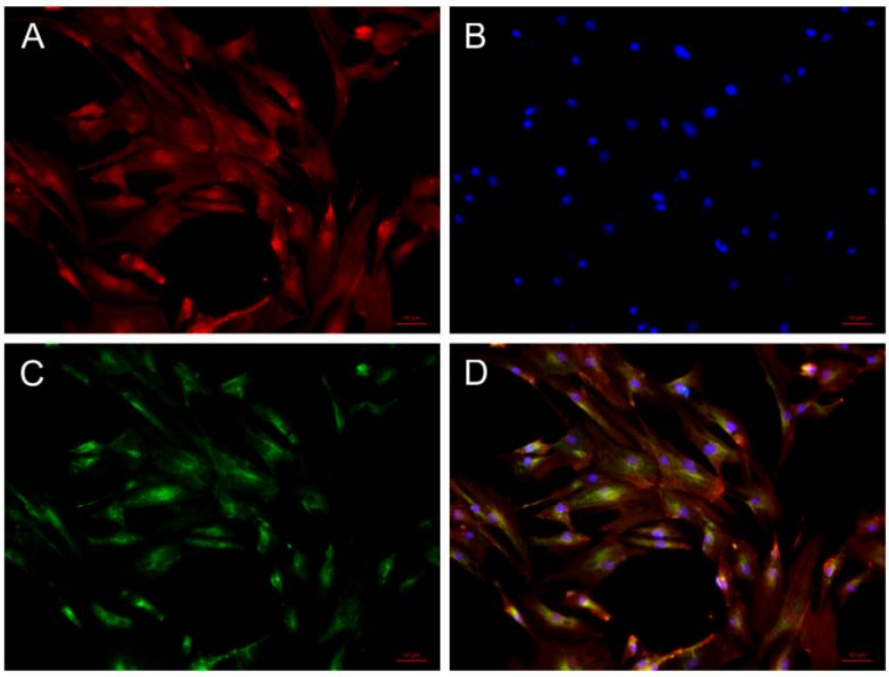

Figure 4.5. Fluorescence images representing alkaline phosphatase (ALP) activity. **A.** Actin-F fibers are visualized applying phalloidin-TRITC staining (red). **B.** Cells nuclei are visualized applying DAPI standing (blue) **C.** ALP protein expression is highlighted by green FITC staining **D.** Merged A., B. and C. image. The scale bars indicate 50 μm.

Therefore, AuNPs@gelatin apart from intrinsic plasmonic properties which succeed in cellular imaging can become promising as well in regenerative medicine due to the enhancement of the cell growth, proliferation and differentiation.

Chapter 5

Design and *in vitro* validation of a new pH-responsive chemotherapeutic nano-system loaded with Doxorubicin

5.1. Chemotherapeutic nano-system characterization

The chemotherapeutic nano-systems were simply realized in one step by mixing the doxorubicin (DOX) solutions at pH 5.5 and pH 10.5 with a purified colloidal AuNPs@gelatin solution in a final drug concentration of 230 μM. Subsequently, we denoted as 5.5DOX-AuNPs@gelatin and 10.5DOX-AuNPs@gelatin the systems prepared in the presence of DOX solution with pH 5.5 and pH 10.5, respectively.

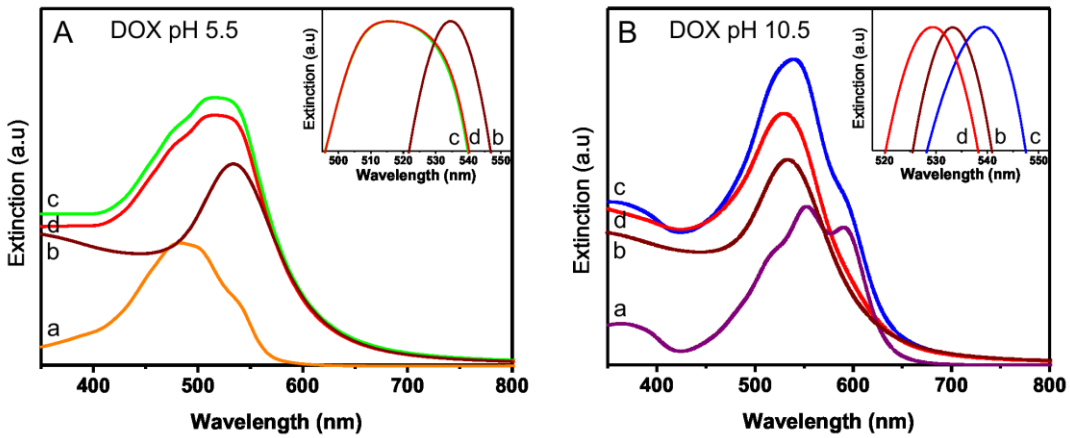

Figure 5.1. a) Absorption spectrum of DOX at **A.** pH 5.5 and **B.** pH 10.5; Extinction spectrum of b) bio-synthesized AuNPs@gelatin, c) DOX-AuNPs@gelatin immediately after their mixture and d) after 24 h incubation. Inset: Normalized spectrum of b) AuNPs@gelatin, DOX-AuNPs@gelatin c) at initial moment and d) after the incubation.

The absorption spectra of DOX at pH 5.5 shows two major bands centered at 290 and 485 nm, corresponding to $\pi \rightarrow \pi^*$ transitions polarized along short and long axis of the DOX molecule, respectively [19]. The main band from 485 nm (Figure 5.1.A spectrum a) is very sensitive to changes occurred in the molecule structure and consequently, at alkaline pH and in the presence of AuNPs@gelatin (Figure 5.1.A and B) this band is shifted to higher wavelengths and reflect the interaction, loading of the drug and formation of 5.5DOX-AuNPs@gelatin and 10DOX-AuNPs@gelatin complexes at pH 5.5 and pH 10.5, respectively. In order to assure a sufficient time for interaction, the drug and AuNPs mixture, were incubated at room temperature for 24h.

The LSPR result is not surprising given that at weak acidic conditions (pH 5.5), DOX molecules are almost fully protonated and interact with the only few negatively charged carboxyl groups of gelatin layer from nanoparticles surface. On the other hand, in alkaline medium at pH

10.5, DOX molecules are deprotonated, carrying a negative charge confirmed by ζ-potential value of -34.9±2.4 mV which promotes the electrostatic interaction with positively charged gelatin layer from the surface of AuNPs. Moreover, the positive ζ-potential value of AuNPs@gelatin (+27.72±1.2 mV) that comes from the amino groups of the gelatin from the surface of nanoparticles switch to a negative value of -24.5±0.8 mV after the interaction with DOX at pH 10.5, which confirms once again the efficient drug loading in alkaline medium.

In order to evaluate the quality of chemotherapeutic systems created,we established that only about 19% of total DOX was loaded onto AuNPs@gelatin in acidic conditions, while a much higher loading of ~70% DOX was achived at DOX pH 10.5. Therefore since the loading efficiency in the alkaline environment is significantly higher than under acidic conditions, next we will investigate only the chemotherapeutic system with higher DOX content, produced at pH 10.5, referred simply as DOX-AuNPs@gelatin.

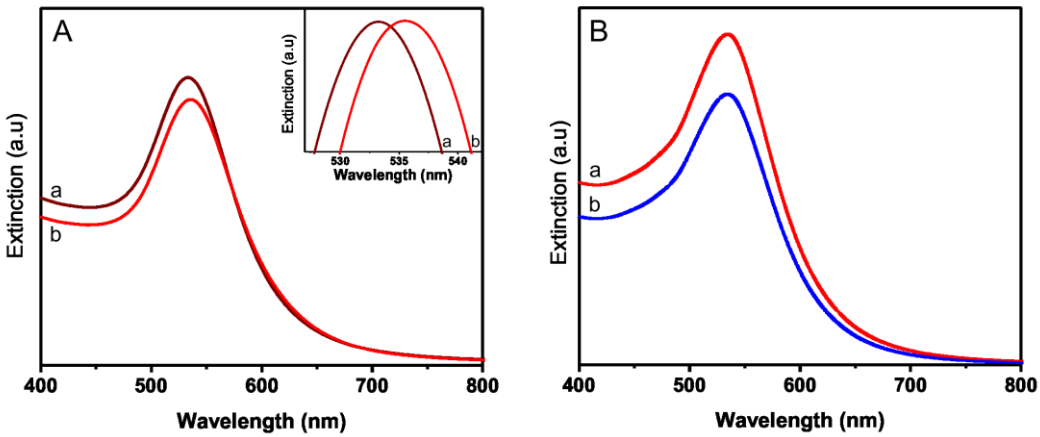

Figure 5.2. A. LSPR spectra of a) AuNPs@gelatin and b) purified DOX-AuNPs@gelatin chemotherapeutic nano-system and **B.** LSPR spectra of DOX-AuNPs@gelatin a) in ultrapure water b) at physiological temperature of 37 °C in 0.9% NaCl solution.

In view of the chemotherapeutic nano-system validation in cellular studies, after the incubation at room temperature for 24 h, the complex was purified by centrifugation (8.000 RPM for 10 min) to remove the unbound drug and redispersed in ultrapure water. As-purified DOX-AuNPs@gelatin exhibit a slight LSPR red-shift (3 nm) compared with unloaded AuNPs@gelatin (Figure 5.2.A) without other optical changes which suggest the stability and successful loading of AuNPs. Moreover, the stability of DOX-AuNPs@gelatin was proved in simulated physiological conditions in 0.9% NaCl solution and at 37 °C (Figure 5.2.B).

5.2. DOX release from chemotherapeutic nano-system

The pH-responsive capability of our DOX-AuNPs@gelatin chemotherapeutic nano-system was evaluated at pH 7.4, 5.3 and 4.6, respectively, to mimic both physiological pH and the acidic environment of cellular organelles and tumour tissue. For this, a small amount of drug loaded nanoparticles was exposed to different buffers and kept under gentle shaking at 37 °C.

The amount of released DOX at predetermined time intervals was measured from the fluorescence emission of the release medium. Fluorescence emission at 593 nm was recorded upon excitation at 485 nm and plotted as a function of time to generate a release profile. Figure 5.3.A shows that the rate and amount of DOX released from DOX-AuNPs@gelatin were highly dependent on the pH of the medium.

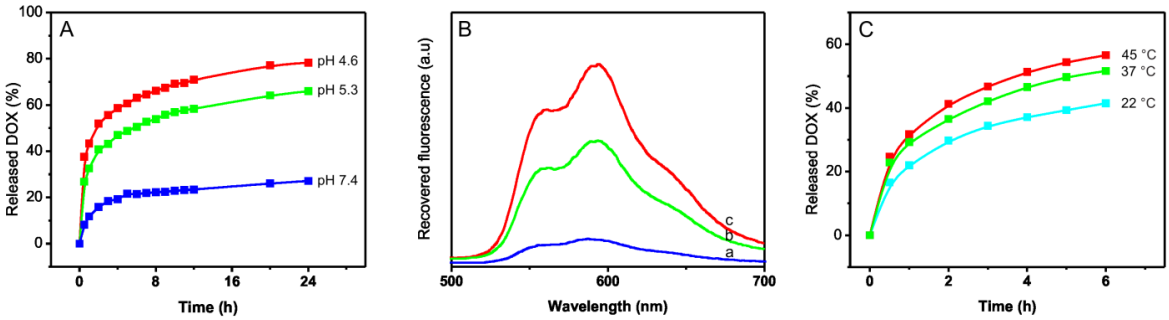

Figure 5.3. A. Effect of pH on DOX release from AuNPs@gelatin at 37 °C, **B**. DOX recovered fluorescence emission after 24 h incubation in buffers at a) pH 7.4, b) pH 5.3 and pH 4.6 and **C.** Effect of temperature on the release behaviour of DOX from AuNPs@gelatin at pH 4.6**.**

Specifically, after 24 h the cumulative released DOX amount reaches about 80% at pH 4.6, which is close to the pH value of tumors and only 25% at pH 7.4, showing a minimal release at physiological pH (Fig 5.3.A,B).

For a particular pH 4.6, the impact of temperature on the release of DOX was further investigated at three different temperatures i.e. room temperature – 22 °C, physiological temperature – 37 °C and hyperthermia temperature – 45 °C. The release profiles are shown in Figure 5.3.C. Compared with the release at 22 °C, it can be clearly seen that a higher temperature imposes a faster DOX release (Figure 5.3.C). This behaviour can be definitely assigned to the gelatin biopolymer component of chemotherapeutic nano-system, which allows a faster DOX release at 37 °C and 45 °C, due to temperature-dependent structure conformation able to increase local mobility in its network by temperature rising.

5.3. Chemotherapeutic nano-system effect on breast cancer cell line MCF-7

5.3.1. Uptake of DOX-AuNPs@gelatin by MCF-7 cells

Figure 5.4 shows the dark-field microscopy images of control – untreated cells and cells treated with DOX-AuNPs@gelatin for 1 h and 24 h, respectively.

Some bluish dots are visible in the control cells due to the characteristic scattering of the intrinsic cellular organelles (Figure 5.4.A) [17]. After 1 h treatment, cells present a limited light-scattering coming from cellular organelles and only a few loaded AuNPs@gelatin can be observed, located mostly at the cellular membrane (Figure 5.4.B). Contrary, after 24 h a strong scattering appears from treated cells which now show inside many bright – orange-reddish spots located at cytosolic level, outside of nuclei.

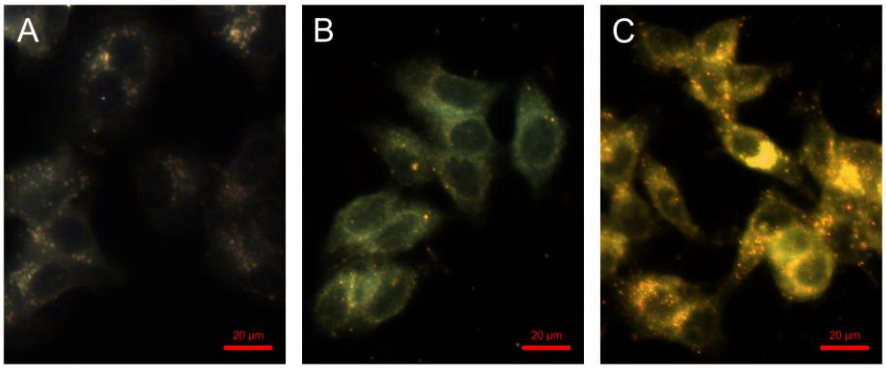

Figure 5.4. Dark-field images of MCF-7 cells **A.** control – untreated and DOX-AuNPs@gelatin treated for **B.** 1 h and **C.** 24 h, respectively.

It is plausible that nanoparticles penetrate the cell membrane trough a process known as endocytosis and reside inside endocytotic vesicles, but outside of nuclei. The observed spots obviously confirm the DOX-AuNPs@gelatin internalization in MCF-7 cells.

5.3.2. Intracellular release of DOX from AuNPs@gelatin

Fluorescence microscopy reveals remarkable differences in the internalization pattern of free DOX and DOX loaded onto AuNPs@gelatin, as can be seen by comparing Figure 5.5 A, B, C and Figure 5.5 D, E, F. The fluorescence signal from cells treated with free DOX appears after only 1h treatment since the free molecules diffuse through cellular membrane and became stronger in time due to drug accumulation which is almost exclusively nuclear.

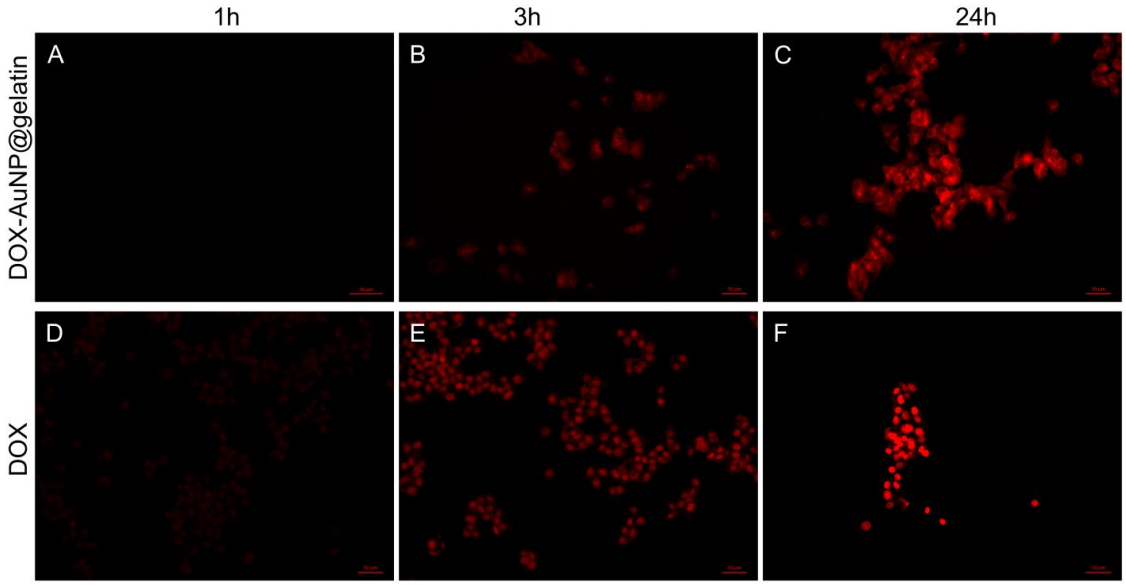

Figure 5.5. Fluorescence images of DOX-AuNPs@gelatin treated cells for **A.** 1 h, **B.** 3 h and **C.** 24 h, and free DOX treated cells for **D.** 1 h, **E.** 3 h and **F.** 24 h, showing the localization of the free DOX and intracellular released DOX at different time intervals. Scale bars show 50 μm.

In contrast, cells treated with DOX-AuNPs@gelatin for 1 h (Figure 5.5.A) show no signal, whereas after 3 h a very low signal is noticed. After 1 h of incubation, the drug loaded gold nanoparticles were not yet internalized, as dark-field imaging show. At 3 h incubation, some drug loaded AuNPs penetrated the cells membrane through endocytosis and a slight red fluorescence from DOX molecules can be observed. This can be attributed to the localization of the chemotherapeutic nano-system within the cells, in endocytic compartments, where the drug release start, triggered by the acidic pH. Here are two states of drug: attached to the metallic surface and located in the biopolymer layer. However, at this time, most of the DOX molecules are still in the close proximity of the AuNPs surface having quenched fluorescence. Judging by the DOX fluorescence intensity we can infer the drug distribution in the cell given that the released DOX migrates to the nucleus to bind DNA. Therefore, after 24 h treatment (Figure 5.5.C), the intensity of the fluorescence signal from released DOX increased, indicating its continuous release. Released DOX is mainly spread through whole cytoplasm but a fluorescence signal can be observed in the cell nuclei, coming from the diffused DOX which reached the nuclei.

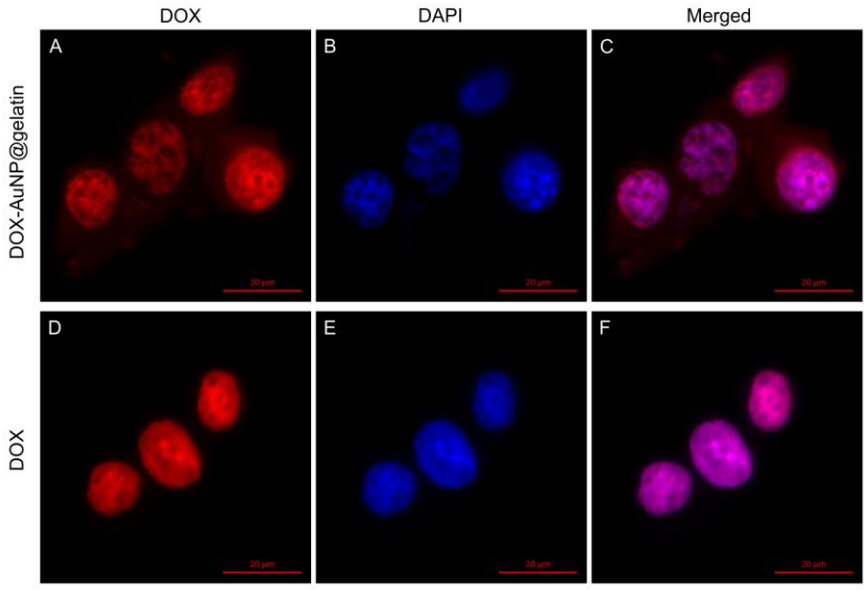

Figure 5.6. Fluorescence images of DOX-AuNPs@gelatin and free DOX treated cells for 48 h, showing the different **A.** intracellular released and **D.** free DOX internalization into nuclei **B.**, **E.** DAPI stained nuclei and **C., E.** merged images

Figure 5.6 show the distribution of DOX in the MCF-7 cells treated for 48 h with either free DOX or DOX loaded onto AuNPs@gelatin which correlated with previous data confirms the different drug internalization and accumulation. Cells treated with free DOX exhibit fluorescence signal only from the nuclei, as DAPI staining protocol confirm. In contrast, cells treated with DOX-AuNPs@gelatin chemotherapeutic nano-system displays a strong fluorescence signal from nuclei and a weak signal from cytoplasm. However, compared with 24 h treated cells, the cytoplasm/nuclei DOX ratio signal is dramatically changed, a higher DOX signal arising from the

nuclei. This observation proves the time-dependent release after a slower DOX-AuNPs@gelatin – cell interaction process, which lead to a sustained drug release, diffusion and subsequent accumulation of DOX in the nuclei.

Next, fluorescence lifetime imaging (FLIM) was used to image both free and Au loaded DOX uptake into cells, given that FLIM is very sensitive to even minor changes in molecules lifetime. But, the fluorescence lifetime of free DOX and DOX loaded onto AuNPs@gelatin in solution were firstly investigated. A monoexponential decay lifetime value of 1.0 ns was recorded from free DOX in solution while after loading onto AuNPs@gelatin, an average lifetime of 1.9 ns was determined for loaded DOX due to the effective gelatin shielding which protects the drug molecules against possible quenchers. These differences in the lifetimes in solution will allow us to take benefit from FLIM to further monitor *in vitro* release from DOX-AuNPs@gelatin.

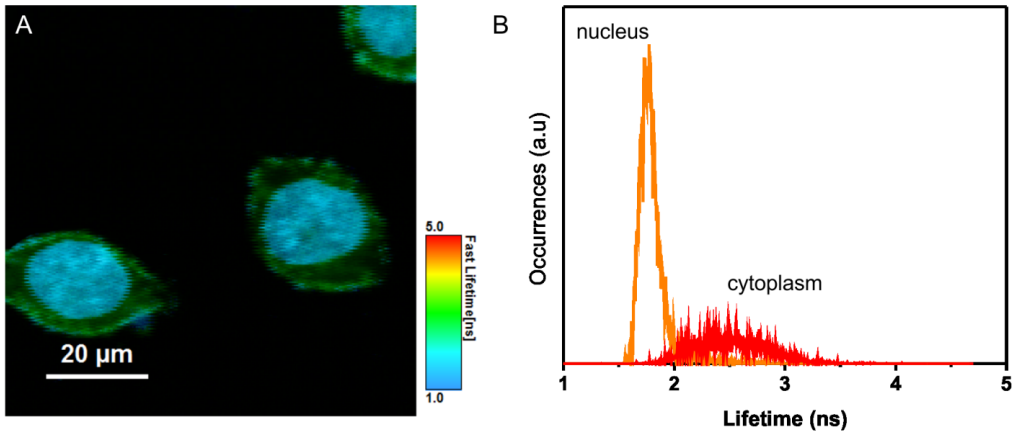

Figure 5.7. A. FLIM image of MCF-7 cells treated with free DOX for 3 h. The color legend presents the corresponding lifetime values ranging from 1 ns to 5 ns. **B.** corresponding lifetime histogram of DOX in cell nucleus and cytoplasm.

Subsequently, FLIM was performed on MCF-7 breast cancer cells treated with free DOX and DOX-AuNPs@gelatin for different periods of time (i.e. 1, 3, 24 and 48 h, respectively). Figure 5.7.A presents the fluorescence lifetime distribution of free DOX in MCF-7 cells after 3 h of incubation. Specifically, we observed that the fluorescence signal is almost entirely nuclear with an increased lifetime value of 1.6 ns (from its corresponding lifetime value in solution) (Figure 5.7.A) attributed to the DOX-DNA intercalation [20] together with a weaker cytoplasmic signal with a longer lifetime value of 2.4 ns (Figure 5.7.B). To note that at 48 h post treatment, all free DOX molecules migrate to the cell nuclei and the fluorescence distribution of DOX signal is exclusively nuclear.

Regarding the case of cells treated with DOX-AuNPs@gelatin, no measurable lifetime signal is detected after 1 h of treatment. After this time, the decays of cytoplasmic signal from cells treated for 3 h fit to a bi-exponential decay with an average lifetime of 4.2 ns. The decay consists of a slow lifetime fraction corresponding to loaded DOX and a fast component attributed to released drug.

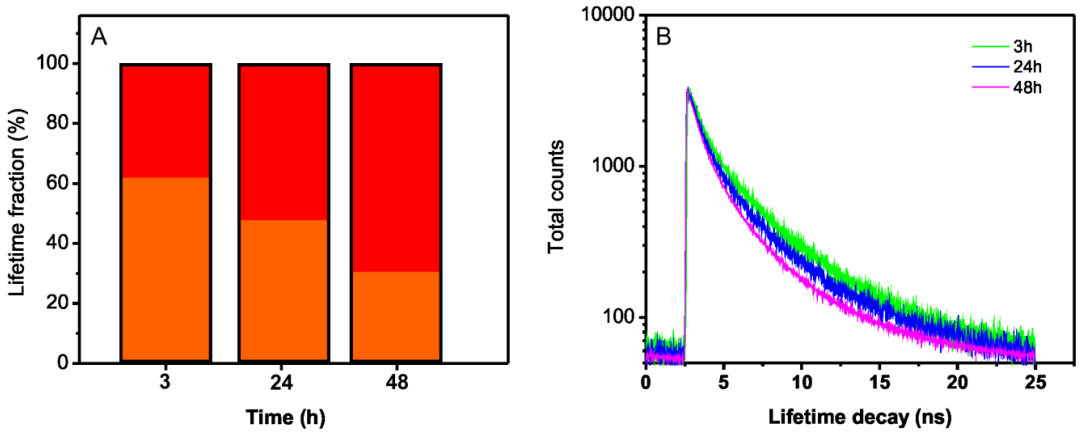

Figure 5.8. A. Values of the fast and slow components in the cytoplasm of cells treated with DOX-AuNPs@gelatin for 3h, 24h and 48h. **B.** The decay curves recorded from MCF-7 cells treated with DOX-AuNPs@gelatin

Nevertheless, over the next several hours, the slow cytoplasmic lifetime (τ_2) fraction was somewhat reduced from ~62% to ~30% in favor of the fraction of the fast component (Figure 5.7). Otherwise, the cells treated for 24 and 48 h illustrates two well defined zones corresponding to the cell nucleus and cytoplasm (Figure 5. 8). Over 48 h treatment, the ratio of the two lifetime fluorescence vary in the cytoplasm inversely proportional with the time of treatment, since the slow lifetime fraction continue to decrease in time whereas the fast lifetime fraction increase. The observed trend obviously reflects the DOX release from AuNPs@gelatin given that the ratio of fast 1.2 ns lifetime (attributed to released DOX) increases in time.

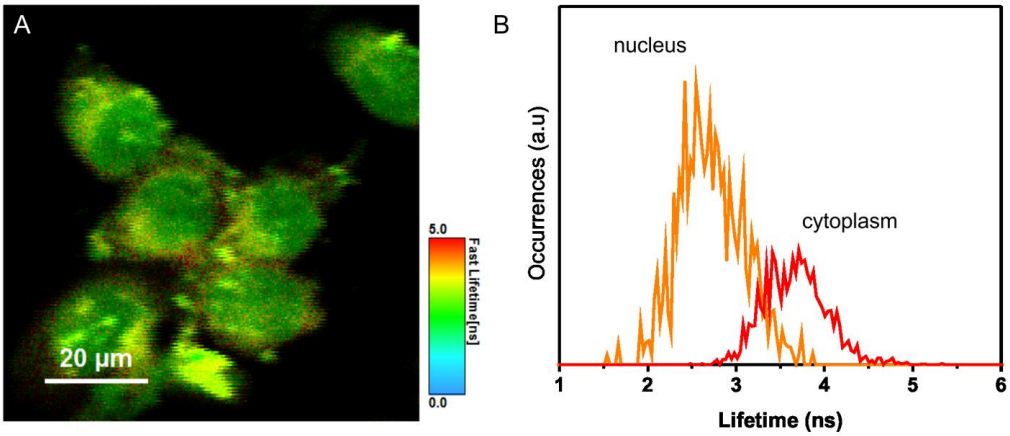

Figure 5.9. A. FLIM images of cells treated with DOX-AuNPs@gelatin for 48 h. The color legend presents the corresponding lifetime values ranging from 0 to 5 ns. **B.** the corresponding lifetime histogram of DOX in cell nucleus and cytoplasm

In parallel, as we mentioned before, the DOX-AuNPs@gelatin nano-system penetrates first the cells, reside in the acidic cellular organelles where the drug release is triggered and then

free drug starts to migrate into the nucleus, where accumulates and bound to DNA strands. The DNA intercalation is also confirmed by the increase of DOX lifetime to 2.4 ns inside of nuclei after 48 h treatment. Hence, we proved once again the different cellular internalization pathways of DOX and DOX-AuNPs@gelatin using FLIM.

As the uptake of DOX-AuNPs@gelatin by the cells was clearly proven by the dark-field images, in the next experiment we examined if enhanced Raman signals can be collected and the nanoparticles can be used as reliable contrast agents for intracellular SERS imaging.

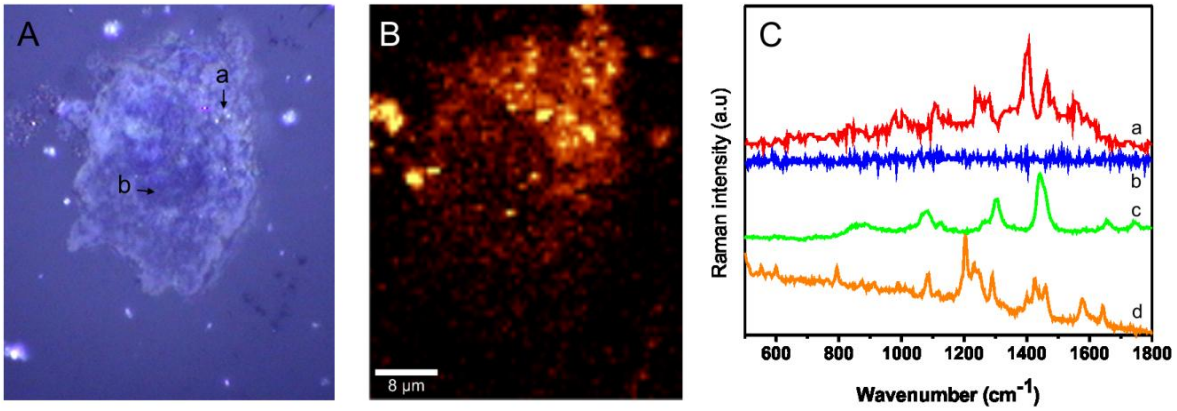

Figure 5.10. A. Optical image of a MCF-7 cell treated with DOX-AuNPs@gelatin for 24h, **B.** SERS map of the same cell, **C.** SERS spectra collected from different point from the treated cell.

Figure 5.10 shows the two-dimensional SERS map of one selected MCF-7 cell incubated with DOX-AuNPs@gelatin for 24h. The univariate spectral image in Figure 5.10.B obtained by plotting the SERS intensity in the spectral range of 600-1700 cm^{-1} resemble closely the basic cellular structure visualized in the bright field microscopic image (Figure 5.10.A.). The bright spots in image A. can be related to metallic nanoparticles known as strong light scatterers relative to background light scattered by subcellular structures as nucleus and mitochondria. Figure 5.10.C spectra a) and b) illustrates two representative SERS spectra recorded from different locations inside a single MCF-7 cell incubated with DOX-AuNPs@gelatin. For comparison, the Raman spectra of the MCF-7 cell and solid DOX are also shown in spectra c) and d) of the same figure. Most of the vibrational bands collected in the presence of DOX-AuNPs@gelatin, can be attributed to the amplified Raman signals of cellular constituents (spectrum a) in Figure 5.10.C corresponding to spot a) in Figure 5.10.A It is obvious that some vibrational bands appear to be spectrally shifted with their intensity ratios modified in comparison with the ordinary Raman bands (Figure 5.10.C spectra a,b and d) due to orientation of biochemical groups relative to the metal surface. We assume that AuNPs@gelatin aggregates inside cells since the gelatin coating is digested by the matrix metalloproteinases (MMP) secreted by MCF-7 cancer cells [21], and therefore promotes the formation of *hot-spots* between interconnected nanoparticles which significantly enhance the Raman signal of biological molecules which come in close vicinity with the agglomerated nanoparticles. However, the SERS enhancement is not limited to the cellular

constituents in the vicinity of the nanoparticles, but is also experienced by DOX molecules. No signal could be detected from regions free of nanoparticles (spectrum b in Figure 5.10.C corresponding to spot b in Figure 5.10.A.).

5.3.3. In vitro cytotoxicity of DOX-AuNPs@gelatin chemotherapeutic nano-system

In this study, MTT assay was performed to test the cytotoxicity of free DOX and AuNPs@gelatin loaded DOX.

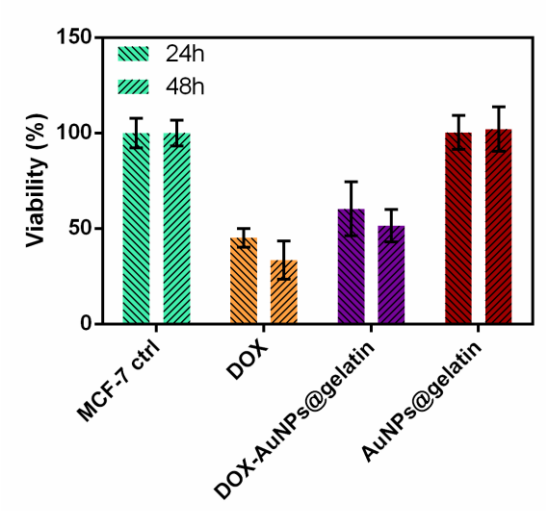

Figure 5.11. Viability of MCF-7 cells treated with DOX and DOX-AuNPs@gelatin in a final concentration of 5 μg/ml drug for 24 and 48 h, together with control untreated cells and AuNPs@gelatin treated, investigated by MTT assay

Figure 5.11 shows the MCF-7 cells time-dependent viability after free DOX, AuNPs@gelatin and DOX-AuNPs@gelatin treatment. As can be seen, after AuNPs@gelatin treatment the cells present excellent viability, comparing with untreated control cells, suggesting that no toxic effect could be recorded. Instead, after the chemotherapeutic treatment with free DOX and DOX-AuNPs@gelatin in a final drug concentration of 5 μg/ml, the half maximal inhibitory concentration (IC_{50}) value for free DOX, the cell viability decreased considerably in a time-dependent manner.

It is not surprising that free DOX showed a higher cytotoxicity than DOX-AuNPs@gelatin, considering their different internalization pathways. AuNPs@gelatin release slowly and sustained DOX after the internalization into cells and only then, the released DOX diffuses to nuclei while free DOX directly penetrates the cell membrane and diffuse to nuclei, as we showed above. Therefore, a high cytotoxicity of the DOX-AuNPs@gelatin chemotherapeutic nano-system, *in vitro*, is another indicator of the efficient DOX release.

Chapter 6
Final conclusions and perspectives

- ✓ We stabilized and functionalized standard citrate-coated gold nanoparticles using gelatin biopolymer
- ✓ We synthesized different size and shaped gold nanoparticles using gelatin
- ✓ We proved that gelatin biosynthesized AuNPs enhance the Osteoblast cells proliferation and differentiation
- ✓ We designed, fabricated and *in vitro* validated a new chemotherapeutic nano-system based on gelatin biosynthesized AuNPs and conventional drug Doxorubicin

Part III
Annexes

Some of the equipments used in my studies are described in this part.

References

[1] R. Asthana, A. Kumar, N.B. Dahotre, Butterworth-Heinemann, 2006.
[2] S. Krol, R. Macrez, F. Docagne, G. Defer, S. Laurent, M. Rahman, et al., Chem. Rev. 113 (2013) 1877–1903.
[3] J.L. Vivero-Escoto, Y.-T. Huang, Int. J. Mol. Sci. 12 (2011) 3888–3927. doi:10.3390/ijms12063888.
[4] W. Cai, T. Gao, H. Hong, J. Sun, Nanotechnol. Sci. Appl. 2008 (2008).
[5] M. Potara, D. Maniu, S. Astilean, Nanotechnology. 20 (2009) 315602.
[6] L. Dykman, N. Khlebtsov, Chem. Soc. Rev. 41 (2012) 2256–2282.
[7] L.A. Dykman, N.G. Khlebtsov, Acta Naturae. 3 (2011) 34–55.
[8] A. Shalviri, G. Raval, P. Prasad, C. Chan, Q. Liu, et al., Eur. J. Pharm. Biopharm. 82 (2012) 587–597.
[9] H.H. Mantsch, D. Chapman, Wiley-Liss, New York, 1996.
[10] A.M. Gabudean, M. Focsan, S. Astilean, J. Phys. Chem. C. 116 (2012) 12240–12249.
[11] M. Potara, M. Baia, C. Farcau, S. Astilean, Nanotechnology. 23 (2012) 055501
[12] A. Miranda, E. Malheiro, E. Skiba, P. Quaresma, P.A. Carvalho, et al., Nanoscale. 2 (2010) 2209–2216.
[13] W. Wu, J. Huang, L. Wu, D. Sun, L. Lin, Y. Zhou, et al., Sep. Purif. Technol. 106 (2013) 117–122.
[14] V.H. Segtnan, T. Isaksson, Food Hydrocoll. 18 (2004) 1–11.
[15] N.G. Parker, M.J.W. Povey, Food Hydrocoll. 26 (2012) 99–107.
[16] E. van den Bosch, C. Gielens, Int. J. Biol. Macromol. 32 (2003) 129–138.
[17] D. Watson, N. Hagen, J. Diver, P. Marchand, M. Chachisvilis, Biophys. J. 87 (2004) 1298–1306.
[18] D. Liu, J. Zhang, C. Yi, M. Yang, Chin. Sci. Bull. 55 (2010) 1013–1019.
[19] M.M. Fiallo, H. Tayeb, A. Suarato, A. Garnier-Suillerot, J. Pharm. Sci. 87 (1998) 967–975.
[20] J.S. Basuki, H.T.T. Duong, A. Macmillan, R.B. Erlich, L. Esser, et al., ACS Nano. 7 (2013) 10175–10189.
[21] J.-H. Xu, F.-P. Gao, L.-L. Li, H.L. Ma, et al., Microporous Mesoporous Mater. 182 (2013) 165–172.